Redox Biology 86 (2025) 103853

Contents lists available at ScienceDirect

Redox Biology

journal homepage: www.elsevier.com/locate/redox

NRF2 deficiency is associated with synaptic alterations and ether-linked phospholipid imbalance in the hippocampus

Daniel Carnicero-Senabre [a,b,c], Mariana A. Barata [d,e], José Jiménez-Villegas [a,b,c], Claudia Guimas Almeida [d], Antonio Cuadrado [a,b,c], Ana I. Rojo [a,b,c,*]

[a] Department of Biochemistry, Medical College, Autonomous University of Madrid (UAM), Madrid, Spain. Instituto de Investigaciones Biomédicas Sols-Morreale (CSIC-UAM), Madrid, Spain
[b] Instituto de Investigación Sanitaria La Paz (IdiPaz), Madrid, Spain
[c] Centro de Investigación Biomédica en Red de Enfermedades Neurodegenerativas (CIBERNED), Madrid, Spain
[d] iNOVA4Health, NOVA Medical School, Universidade Nova de Lisboa, Lisboa, Portugal
[e] Centre for Discovery Brain Sciences, Hugh Robson Building, George Square, University of Edinburgh, Edinburgh, EH8 9XD, Scotland, UK

ARTICLE INFO

Keywords:
NRF2
Synapses
Lipidomics
Ether-lipids
6-MSITC

ABSTRACT

Synaptic loss is a key factor in the cognitive decline observed during aging and in neurodegenerative diseases such as dementia, where synaptopathy plays a central role in hippocampal dysfunction. In this study, we investigated the role of NRF2, a master regulator of cellular homeostasis, in maintaining synaptic integrity. We assessed synaptic contacts both *in vitro* and *in vivo* and found that NRF2 deficiency leads to a significant reduction in vGLUT1 levels, accompanied by a decrease in the number of synaptic contacts. Because synapses are subject to highly dynamic membrane remodeling processes, we analyzed the lipid composition of hippocampi and synaptosomes from NRF2-deficient and wild-type mouse littermates. Our results revealed an accumulation of ether-linked phospholipids in NRF2-deficient mice. When primary neuronal and organotypic cultures were exposed to an ether-lipid precursor, synaptic density decreased. By contrast, the NRF2 activator 6-(methylsulfinyl)hexyl isothiocyanate (6-MSITC or hexaraphane) prevented synaptic loss. Although ether lipids are abundant components of neuronal membranes, their specific role in synaptic function and in age-related loss of homeostatic balance remains poorly understood. This study is the first to demonstrate that NRF2 plays an essential role in preserving synaptic homeostasis through lipid metabolism, suggesting its relevance in the context of aging and neurodegenerative diseases.

1. Introduction

While subtle cognitive decline with discrete synaptic loss is a feature of normal aging, advanced neurodegenerative conditions are characterized by widespread synaptic and neuronal degeneration. Synaptic loss in the hippocampus is linked to dementia, in which structural and functional synaptic alterations, collectively known as synaptopathies, play a key role in the cognitive decline characteristic of these disorders [1,2].

Glycerophospholipids are the predominant lipid class in neural cell membranes, with ether lipids particularly abundant [3,4]. Ether lipids are characterized by the presence of an ether bond at the *sn*-1 position of the glycerol backbone, with choline and ethanolamine being the most represented polar head groups. They are broadly divided into alkyl-lipids, which contain a saturated alkyl ether linkage, and alkenyl-lipids (also called vinyl-lipids or plasmalogens), which have a vinyl-ether bond featuring a double bond adjacent to the ether oxygen. Alkyl lipids are chemically stable and inert, whereas vinyl lipids are more reactive due to the presence of the vinyl-ether bond. Both types contribute to key membrane properties such as fluidity, lipid raft formation and stability, and act as reservoirs for second messengers. Additionally, they are involved in transmembrane protein function, cholesterol transport, vesicular trafficking, membrane fusion, and G-protein-mediated signal transduction [5–7]. Notably, an antioxidant role has been attributed to plasmalogens, due to their unique structural feature since the vinyl-ether bond is highly susceptible to oxidation by reactive species, such as reactive oxygen species (ROS) and hypochlorous acid, allowing them to act as scavengers that protect unsaturated

* Corresponding author. Instituto de Investigaciones Biomédicas "Sols-Morreale", C/Arturo Duperier, 4, 28029, Madrid, Spain.
E-mail address: airojo@iib.uam.es (A.I. Rojo).

https://doi.org/10.1016/j.redox.2025.103853
Received 2 June 2025; Received in revised form 26 August 2025; Accepted 29 August 2025
Available online 30 August 2025

membrane lipids and lipoproteins from oxidative damage [8].

Lipidomic analyses indicate an inverse correlation between ether lipid levels and genetic peroxisomal disorders as well as with prevalent conditions such as obesity, prediabetes, type 2 diabetes mellitus, cardiovascular disease, cancer, and Alzheimer's disease [5,6,9,10]. Interestingly, these pathological conditions are commonly linked to elevated oxidative stress, suggesting a potential mechanistic role for ether lipids [11,12]. From an aging perspective, the ether lipid profile appears to be optimized for exceptional human longevity, since centenarians exhibit higher plasma levels of alkyl-phosphatidylcholine (PC–O) and reduced levels of alkenyl-phosphatidylethanolamine (PE-P) [13]. However, the role of ether lipids in synapses and their connection to age-related loss of homeostatic responses remains poorly understood.

In this study, we addressed this issue in the context of NRF2 (Nuclear factor erythroid 2-related factor 2) deficiency, as NRF2 is the master regulator of homeostatic responses. NRF2-driven gene expression provides a robust cytoprotective transcriptional program that regulates ROS signaling, inflammation, and lipid metabolism to maintain physiological homeostasis [14]. Notably, NRF2 activity declines with age [15] and is mislocalized to the nuclear periphery in Hutchinson-Gilford progeria syndrome, characterized by premature aging [16]. Moreover, male mice treated with an NRF2 activator exhibit an extended lifespan [17]. Importantly, the NRF2-deficient mouse brain recapitulates biological pathway alterations found in elderly humans [18,19]. Several studies have linked NRF2 to synaptic function and lipid metabolism, though its role in lipid composition remains unexplored. It has been shown that NRF2 deficiency downregulates key synaptic proteins such as PSD95, synapsin I, and synaptophysin, correlating with learning and memory deficits. NRF2-null mice display fewer synaptic vesicles, reduced spine density, and impaired bilateral hippocampal connectivity [19–22]. Consistent with this, we previously demonstrated that NRF2-KO mice exhibit a decreased electrophysiological response to tetanic stimulation, concomitant with impairments in the neurogenic niche of stem cells in the dentate gyrus [24].

This study employs a lipidomic analysis on NRF2-knockout brains and synapses, introducing a new experimental model of alkyl-lipid synaptopathy. It establishes an essential role for NRF2 in the regulation of synaptic lipid composition and integrity.

2. Material and methods

Transgenic mice. Colonies of NRF2-KO mice and NRF2-WT littermates were established from founders kindly provided by Dr. Masayuki Yamamoto (Tohoku University Graduate School of Medicine, Sendai, Japan) [25]. Animals were housed at room temperature under a 12 h light-dark cycle. Food and water were provided *ad libitum*. Animals were cared for according to a protocol approved by the Ethical Committee for Research of the Autonomous University of Madrid following institutional, Spanish and European guidelines (Boletín Oficial del Estado (BOE) of March 18, 1988; and 86/609/EEC, 2003/65/EC European Council Directives). Once the experimental schedule was completed, animals were anesthetized with 8 mg/kg ketamine and 1.2 mg/kg xylazine and perfused with PBS. The brains were divided sagittally, and the right hemispheres were post-fixed in 4 % paraformaldehyde (Sigma-Aldrich, St. Louis, MO, USA, 158127) for 16 h or 3 % glyoxal (TCI, Zwijndrecht, Belgium, G0152) for 48 h and cryoprotected by soaking in 30 % sucrose solution in phosphate buffer until they sank. The left hemispheres were rapidly dissected and frozen for biochemical analysis.

Untargeted lipidomics. Sample preparation and lipidomics analysis were performed by an external service (oloBion SL, OMICS life lab, Barcelona, Spain; https://www.olobion.ai/). The samples were homogenized with cold methanol using a milling ball. Then MTBE was added, and the samples were shaken and centrifuged. For the lipidomic profiling, the upper organic phase was collected, evaporated, and resuspended using methanol with an internal standard, shaken, centrifuged, and used for LC-MS analysis. The lipids were separated on a Water ACQUITY UPLC BEH C18 column maintained at 65 °C by and coupled to a ZenoTOF 7600 system (SCIEX). The sample was injected at 5 μL in ESI positive and negative mode. Lipidomic data from positive and negative ion modes were merged by lipid identity. For lipids detected in both modes, the most intense signal was kept to avoid redundancy, ensure consistency and improve data quality for analysis. The peak intensity area was normalized using internal deuterated standards. For lipid identification, the data was processed by oloMAP 2.0 according to Ref. [26]. Lipids identification with odd chain carbon numbers should be considered microbial contamination or present in the media used for cell growth. The uncorrected p-value threshold is set to 0.05, and the log2(FC) ranges to (−0.5, 0.5).

***In silico* analysis of lipid reaction pathway activity.** To perform *in silico* pathway analysis for lipid species, the metabolites names identified in the untargeted lipidomics study were converted to BioPAN [27] compatible names using LipidLynxX [28]. Metabolites whose names could not be converted to BioPAN-compatible names were discarded for further analysis. A matrix with individual lipid abundances per sample was submitted to the BioPAN online tool with default parameters and Z-scores for the reactions for the different lipids were retrieved at the lipid subclass and fatty acid levels. Z-scores across different reactions were calculated using a custom Python script by summing the Z-scores of individual reactions and dividing the sum by the square root of k-1, where k is the number of lipids involved in that chain of reactions. This criterion is identical to the one used in BioPAN. A directed network of lipid reactions was created using Cytoscape [29].

Culture of primary neurons. As previously, cortical and hippocampal pieces were obtained from E16-E18 embryos [30]. Briefly, after dissection, tissue was incubated in HBSS (Hank's Balanced Salt Solution, Gibco, Waltham, MA, USA, 15420614) with 10 % TrypLE Express (Gibco, Waltham, MA, USA, 11538856) and left for 15 min at 37 °C to allow for light digestion. After that, pellets were washed with HBSS and mechanically dissociated with DMEM – high glucose (Dulbecco's modified Eagle's medium with high glucose; Sigma-Aldrich, San Luis, MO, USA; D5648) supplemented with 10 % fetal bovine serum (FBS; Biowest, Nuaillé, France, S1400) and 80 μg/mL gentamycin (Normon Laboratories, Tres Cantos, Spain). Cells were then pelleted at 3000 rpm for 5 min and resuspended in a supplemented DMEM medium. 3–24 h after plating, the medium was fully replaced with BrainPhys with 2 % SM1 (StemCell, Vancouver, BC, Canada, 05792) and 80 μg/mL gentamycin. This media allowed for a more physiological differentiation than the traditional Neurobasal, with minimal glial presence, especially in coverslips. Neurons were used at 15 DIV and treated the day before with either 9 μM 6-MSITC, provided by LKT Labs (Minnesota, USA); 9 μM 1-*O*-hexadecyl-*sn*-glycerol (HG, Santa Cruz Biotechnology Inc., California, USA, sc-202394) or 9 μM DL-α-palmitin (DP, Sigma-Aldrich, MO, USA, M1640). Both lipids were first dissolved in ethanol and further diluted in cell medium until the ethanol concentration was lower than 0.1 %.

Organotypic slice preparation. Organotypic slices were prepared as previously described with slight modifications [31]. Briefly, hippocampal slices were obtained from adult NRF2-WT mice by extracting the hippocampus in dissection buffer, consisting of HBSS and 80 μg/mL gentamycin. Hippocampi were cut into 300 μm-thick slices and cultured for one week on inserts (Millipore, Merck, Rahway, NJ, USA, PICM050). Culture media (50 % DMEM, 25 % HBSS, 25 % horse serum, 80 μg/mL gentamycin and 2 mM L-glutamine) was changed once every 3–4 days.

Analysis of mRNA levels. Total RNA extraction, reverse transcription, and quantitative polymerase chain reaction (qRT-PCR) were done as detailed in Ref. [32]. Primer sequences are shown in Sup. Table 2. To ensure that equal amounts of cDNA were added to the PCR reaction, *Actb*, *Gapdh* and *Tbp* housekeeping genes were amplified. Data analyses were based on the ΔΔCT method, normalizing the raw data by the geometric mean of the housekeeping genes *Actb*, *Gapdh* and *Tbp* (Applied Biosystems). All PCR amplifications were performed in at least triplicate experiments.

Immunoblotting. Cells were washed with cold PBS and homogenized in lysis buffer (50 mM Tris pH 7.6, 400 mM NaCl, 1 mM EDTA, 1 mM EGTA and 1 % SDS). Samples were heated at 95 °C for 15 min and sonicated (100 % amplitude, 1 cycle, 5 s) (Hielscher Ultrasonics GmbH, Teltow, Germany, UP100H). Protein quantification was performed with the DC™ Protein Assay (Bio-Rad, Hercules, CA, USA, 5000112), and protein loading buffer (50 mM Tris-HCl pH 6.8, 2 % SDS, 0.1 % bromophenol blue, 10 % glycerol, 150 mM β-mercaptoethanol) was added. Samples were boiled at 95 °C and cellular debris was cleared with centrifugation. Proteins were resolved using SDS-PAGE and transferred to 0.45 μm pore size Immobilion-P membranes (Millipore, Burlington, MA, USA, IPVH00010). For immunoblotting, membranes were hydrated in methanol, washed in TTBS (20 mM Tris-HCl pH 7.5, 150 mM NaCl and 0.1 % Tween 20) buffer and blocked with 5 % non-fat dry milk in TTBS. Membranes were incubated with the appropriate dilution of the primary antibodies (Sup. Table 1) in 0.4 % BSA or 2.5 % non-fat-dry milk and 0.02 % azide overnight, washed and incubated with 1:10,000 dilution of secondary antibodies coupled to horseradish peroxidase in 0.4 % BSA TTBS for 1 h. Proteins were detected by enhanced chemiluminescence (AmershamTM ECL™ Select Western Blotting Detection Reagent, GE Healthcare, Chicago, IL, USA, GERPN2235) and quantified using imaging software ImageJ (Fiji).

Immunofluorescence. Primary neurons were seeded on sterile coverslips (35,000 cells per well) pretreated with poly-D-Lysine (0.1 mg/mL, Sigma-Aldrich, San Luis, MO, USA; P1024). After the indicated treatments the cells were washed with PBS and fixed in 4 % paraformaldehyde and 4 % sucrose (Sigma-Aldrich, San Luis, MO, USA; 158127) for 15 min. After PBS washes, cells were permeabilized with PBS containing 0.3 % Triton X100 (Sigma-Aldrich, San Luis, MO, USA; ID X100) for 5 min and blocked in PBS containing 0.3 % Triton X100 with 2 % fetal bovine serum and 1 % bovine serum albumin (NZYTech, Lisboa, Portugal; ID MB046) for 1 h. Primary antibody (Sup. Table 1) was diluted in blocking buffer and incubated for 1 h. After washing primary antibody with PBS 1x, corresponding secondary antibodies conjugated with Alexa Fluor dyes (Invitrogen, Waltham, MA, USA) and DAPI (4′-6-diamino-2-phenylindole, Invitrogen, Waltham, MA, USA, 1306) were incubated for 1 h at room temperature. Coverslips were mounted using ProLong™ Gold Antifade Mountant (Invitrogen, Waltham, MA, USA; P36930) and dried for 24 h before visualization.

Brain immunohistochemical staining (IHC). Sagittal series of 30-μm-thick sections were obtained in a freezing microtome and stained as indicated previously [32]. For organotypic slices, sections were fixed with 3 % glyoxal, after washing, permeabilized (0.3 % Triton X-100 in 0.1 M phosphate buffer) and blocked (0.3 % Triton X-100/5 % BSA in 0.1 M phosphate buffer) were incubated with the primary antibody for 16h at 4 °C. The primary antibodies used are described in Suppl. Table 1. The corresponding secondary antibodies used were conjugated to Alexa Fluor. Coverslips were mounted using ProLong™ Gold Antifade Mountant (Invitrogen, Waltham, MA, USA; P36930) and dried for 24 h before visualization. Images from primary, organotypic or brain slices were acquired using the LSM710 spectral microscope confocal (Zeiss, Germany), Stellaris 8 Tau STED (Leica, Germany) or AiryScan-LSM 980 confocal microscope (AiryScan 2, Zeiss), respectively.

Synaptosome, synaptic vesicle and synaptosomal membrane isolation. Samples were homogenized with a pestle in ice-cold buffer 1 (0.32 M sucrose, 10 mM HEPES, 1 mM EDTA, 1 mg/ml leupeptin and 1 mM PMSF) [33]. The homogenate was centrifuged (10 min, 1000g) and the post-nuclear supernatant (input) was saved and centrifuged (15 min, 10 000g) to generate a pellet that contains crude synaptosomes (Syn). Syn was resuspended in 500 μL of 4 mM HEPES, 1 mM EDTA, pH 7.4 and centrifuged (15 min, 10 000g) generating the washed synaptosome fraction, which was lysed by hypoosmotic shock in ice-cold buffer 2 (20 mM HEPES, 100 mM NaCl, 0.5 % Triton X-100, 1 mM phenylmethylsulfonyl fluoride, 1 g/ml leupeptin), homogenized with a pestle and left in a rotating wheel for 30 min to ensure complete lysis. The lysate was further centrifuged (30 min, 21 000g) to generate a supernatant that contains crude synaptic vesicles (SV) and a pellet that contains synaptosomal membranes (SM). SM fraction was resuspended in RIPA buffer. All steps were performed at 4 °C.

Endocytosis analysis by FM4-64 fluorescence probe. Primary neurons at 14 DIV were incubated with 10 μM of the lipophilic dye FM 4-64-Fx (Thermo Fisher Scientific, San Jose, CA, USA, F34653) for 90 s in a high-potassium solution [30]. Neurons were washed twice with a low-calcium solution for 30 s, fixed for 10 min in 2 % PFA, and mounted for imaging with ProLong™ Gold Antifade Mountant.

Calcium imaging by Fluo-4 AM fluorescence probe. Primary neurons at 14 DIV were incubated with 5 μM Fluo-4 AM (Invitrogen, Waltham, MA, USA F14201) and 0.01 % Pluronic® F-127 (Sigma-Aldrich) for 30 min in BrainPhys Imaging (BPI) (Stemcell, Vancouver, BC, Canada, 05796) at 37 °C. After that, cells were washed with BPI three times and taken to the microscope, where they remained at 37 °C in a coupled chamber. Images were recorded every 5 s and 65 mM KCl was used to stimulate calcium waves. Fluorescence levels were quantified with Fiji, by measuring three same-sized ROIs/conditions, and statistical analysis was performed by the $\Delta F/F_0$ method [34].

Cell viability. In live cells but not in dead ones, the tetrazolium ring of 3-(4,5-dimethylthiazol-2-yl)-2,5-diphenyltetrazolium bromide (MTT, Sigma-Aldrich, St. Louis, MO, USA, 475989) can be reduced by active dehydrogenases to produce a formazan precipitate. At the end of the experiments, cells were washed three times with phosphate-buffered saline (PBS) followed by adding MTT (0.125 mg/ml) and incubating for 1 h at 37 °C. The media was removed and DMSO was added to each well to dissolve the formazan precipitate for 30 min, thereby determining the relative number of living cells. An aliquot (100 μl) of the supernatants was analyzed in 96-well multiwell plates at 550 nm in a VERSAmax™ microplate reader (Molecular Devices).

Quantitative imaging analysis. Image analysis was carried out using Fiji (ImageJ 1.53, https://fiji.sc/). For quantification of colocalization of PSD95-vGLUT1/vGAT-gephyrin puncta in primary neurons and brain tissue (number, size and mean fluorescence), the "ComDet v.0.5.5" plugin was used for segmentation and colocalization, considering maximum distance between objects less than 5 pixels. For primary neurons, neurite ROIs were outlined using the "rotated rectangle" tool. All parameters were presented as the percentage of the control situation. The quantification of NR2B puncta and C1q/vGLUT1 colocalization were also analyzed using the same plugin. For primary neurons, analysis was carried out on three independent cultures from three different sets of embryos and an average of 10 neurons/experiment were analyzed.

Statistical analysis. Unless otherwise indicated, all experiments were performed at least 3 times and all data presented in the graphs are the mean of at least 3 independent samples. Data are presented as mean ± SD (standard deviation) or mean ± SEM (standard error of the mean) as stated in the figure legend unless indicated otherwise. Statistical differences between groups were assessed using GraphPad Prism 8 by one analysis of variance (ANOVA), using Bonferroni post-hoc test, or Student's unpaired *t*-test (*** indicates p values < 0.001, **$p < 0.01$ and * $p < 0.05$).

3. Results

The density of glutamatergic synapses is reduced in neurons from NRF2-null mice. To elucidate the role of NRF2 in the maintenance of synapses, we first established cortical/hippocampal primary neuronal cultures from NRF2-WT and NRF2-KO. Characterization of the differentiation process and evaluation of NRF2 basal activity are shown in Supp. Fig. 1. To quantify GABAergic synapses, presynaptic and postsynaptic compartments were labeled with the vesicular transporter of GABA (vGAT, green) and the postsynaptic Gephyrin protein (magenta), respectively, with co-localizing puncta (white) representing inhibitory synapses (Fig. 1A and Suppl. Fig. 2A). As shown in the immunofluorescence analysis depicted in Fig. 1B, the density (number of co-localizing puncta/50 μm^2) of GABAergic contacts was similar in both

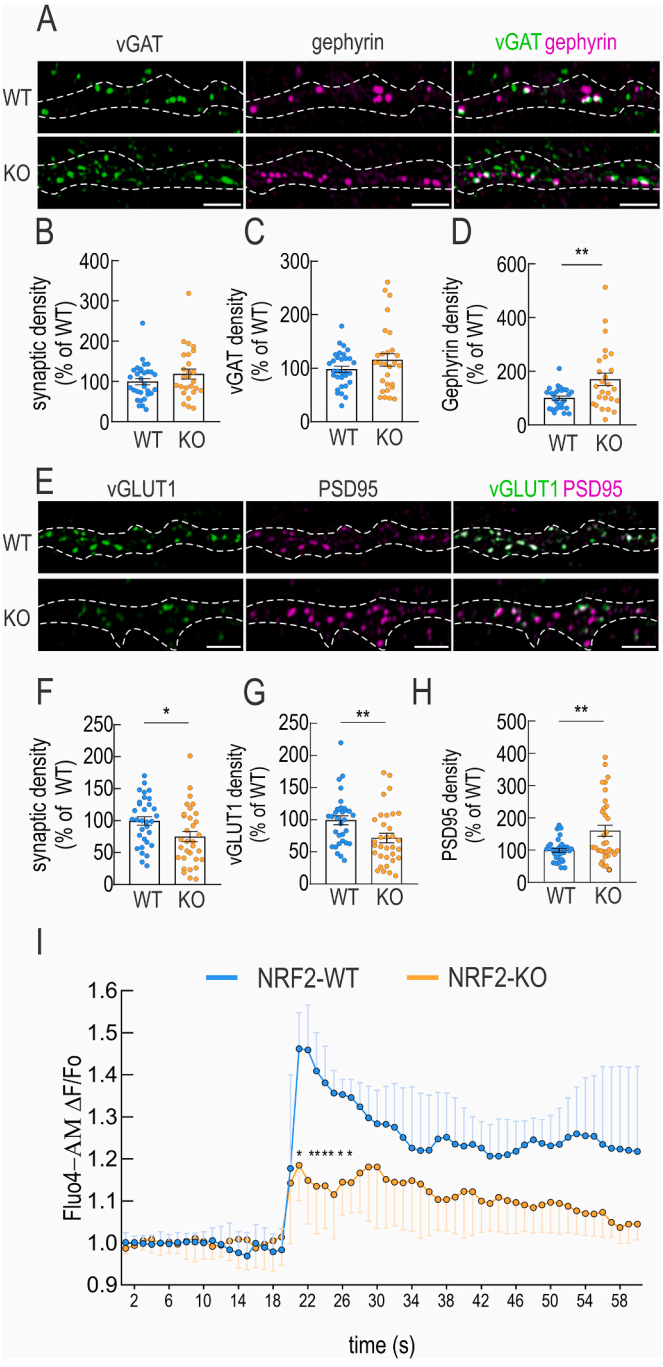

(caption on next column)

Fig. 1. ***The number of glutamatergic contacts is reduced in primary neurons from NRF2-KO compared to NRF2-WT mice.*** A, confocal analysis of double immunofluorescence with anti-vGAT (green) and anti-Gephyrin (magenta) antibodies in primary hippocampal/cortical neurons from NRF2-WT and NRF2-KO mice maintained for 14 days *in vitro* (DIV). The scale bar corresponds to 5 μm. Dotted lines represent neurite outlines. B, quantification of colocalization between vGAT and Gephyrin staining expressed and represented as synaptic density (number of puncta per 50 μm^2) and % of WT. C and D, quantification of vGAT or Gephyrin density (number of puncta per 50 μm^2), respectively. E, confocal analysis of double immunofluorescence with anti-vGLUT1 (green) and PSD95 (magenta) antibodies in primary hippocampal/cortical neurons from NRF2-WT and NRF2-KO mice maintained for 14 DIV. The scale bar corresponds to 5 μm. Dotted lines represent neurite outlines. F, quantification of colocalization between vGLUT1 and PSD95 staining expressed and represented as synaptic density and % of WT. G and H, quantification of either vGLUT1 or PSD95 density (number of puncta per 50 μm^2), respectively. The number of positive puncta was derived from 3 independent experiments with an average of 30 neurons per genotype and experiment. All data are mean ± SEM. Primary hippocampal/cortical neurons from NRF2-WT and NRF2-KO mice maintained for 14 DIV, were loaded with the calcium reporter Fluo-4 AM (10 μM) and submitted to 65 mM KCl treatment. I, quantification of Fluo-4 AM fluorescence intensity normalized by the basal fluorescence value ($\Delta F/F_0$) analyzed for 60 s. Data are mean ± SD (n = 3/genotype). Statistical analysis was performed by using unpaired *t*-test. *p < 0.05; **p < 0.01 vs. WT.

genotypes. In the presynaptic compartment, the vGAT number also did not differ between genotypes (Fig. 1C), despite the slight increase in the density of Gephyrin (Fig. 1D). There was a slight reduction in the intensity and size of vGAT positive puncta (Suppl. Fig. 2B and 2C, respectively) in NRF2-KO compared to control neurons. Conversely, small variations in the intensity and size of Gephyrin puncta were detected (Suppl. Fig. 2D and 2E, respectively).

Employing a similar approach but labeling glutamatergic pre- and postsynaptic compartments with the vesicular transporter of glutamate, vGLUT1 (green) and the postsynaptic protein, PSD95 (magenta) (Fig. 1E and Suppl. Fig. 2F), we evidenced that glutamatergic contacts were significantly reduced in neurons from NRF2-null compared to those from control mice (Fig. 1F.). Deeper analysis of the density, intensity and size of the vGLUT1 and PSD95 puncta evidenced a significant reduction in the number of vGLUT1 positive puncta in neurons deficient for NRF2 expression (Fig. 1G and Supp Fig. 2 G-K). Remarkably, although there was an increase in the size (Supp. Fig. 2K) and number (Fig. 1H) of PSD95 puncta, the overall number of glutamatergic contacts was reduced upon NRF2 deficiency.

Since neurons deficient in NRF2 expression exhibited a reduced density of vGLUT1 and electron microscopy studies on NRF2-deficient animals have shown that presynaptic compartments have a reduction in the number of vesicles [35], we analyzed whether there could be any alteration in endocytic dynamics using FM 4–64 [36]. Neurons were incubated with the dye in a high-potassium solution to induce synaptic vesicle release and compensatory endocytosis, with active synapses being labeled with FM 4–64, and then washed in a low-calcium solution to remove non-internalized FM 4–64. The lack of differences in FM 4–64 uptake between genotypes suggests a compensatory mechanism in NRF2-null neurons or that vGLUT1 deficiency is unrelated to the analyzed endocytic mechanism (Suppl. Fig. 3A–D). Additionally, we compared the expression pattern of NR2B, the NMDA receptor subunit, between NRF2-null and control neurons. In NRF2-deficient neurons, we detected a modest increase in the number of NR2B-positive puncta, and a slight reduction in their intensity and size (Supp. Fig. 3E–H). Glutamate receptors are primarily calcium channels; therefore, we evaluated their functionality by measuring if calcium rises using Fluo 4-AM. As expected, in response to a depolarizing stimulus (65 mM KCl), Fluo 4-AM fluorescence abruptly increased 1.2-fold in both NRF2-WT and -KO neurons at 20 s. In contrast, 2 s later, the calcium levels in WT neurons continued to rise, reaching a 1.4-fold increase, while KO neurons failed to respond further, maintaining stable fluorescence until the

end of the recording (Fig. 1I). These data suggest that NRF2 plays an important role in maintaining the proper number of glutamatergic contacts to support neuronal activity.

The lipidic landscape of the hippocampus is dysregulated by NRF2 deficiency. Since the hippocampus is a key anatomic formation for synaptic plasticity and encoding of memories, untargeted lipidomics was performed on hippocampal samples from NRF2-knockout (NRF2-KO) vs. wild-type (NRF2-WT) mice (Supp. Table 3). An initial principal component analysis (PCA) plot was generated with data from hippocampi to check trends and to ensure the grouping of all samples (PC1, 33.7 %; PC2, 24.8 %) (Supp. Fig. 4A). Evaluation of the lipidomic profiles employing partial least squares discriminant analysis (PLS-DA) revealed that NRF2-KO and WT mice appear to be separated sample groups (Fig. 2A and Supp. Table 4). We evaluated 645 distinct lipid species, grouped into seven categories (Supp. Fig. 4B), through network analysis of lipid pathway activity using BioPAN [27]. This exploration

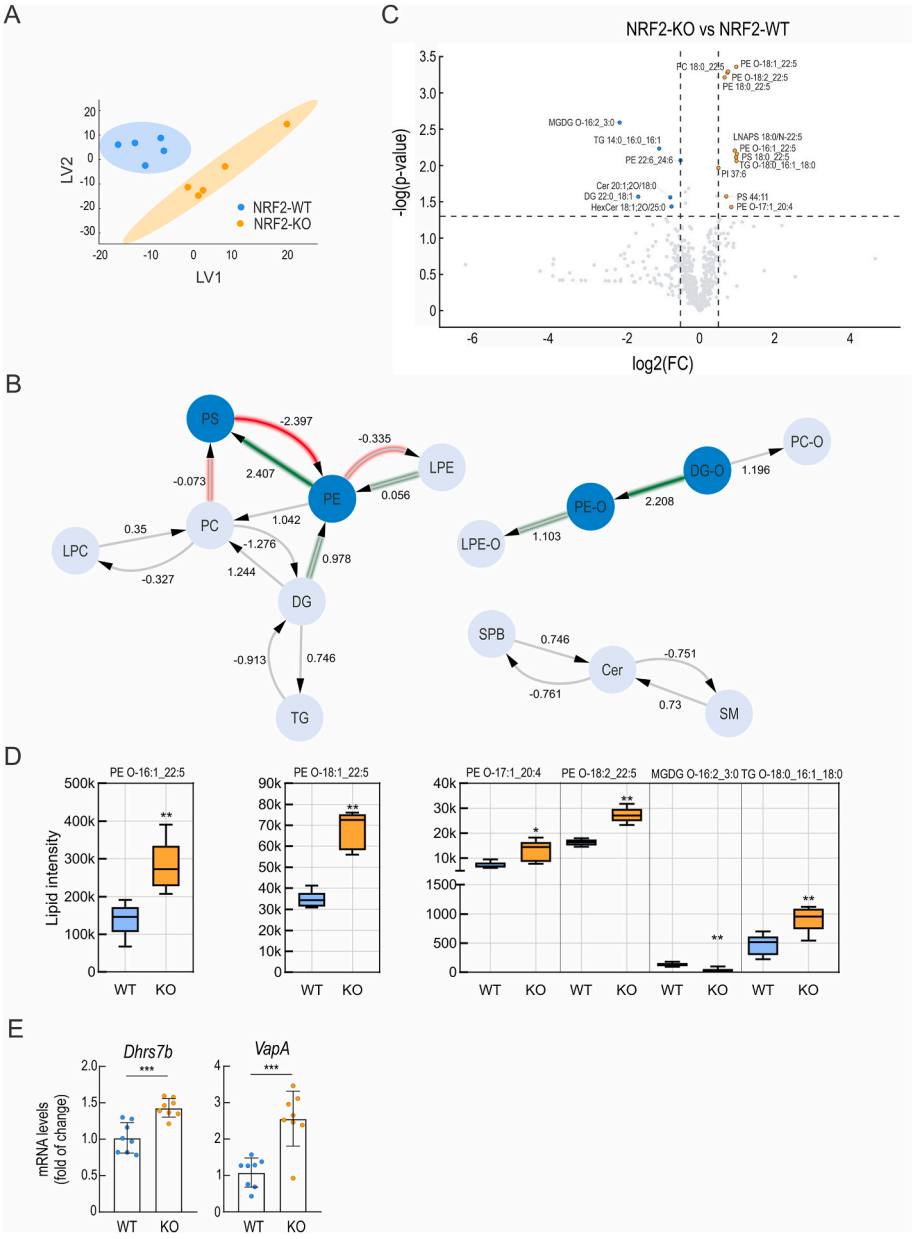

Fig. 2. ***NRF2-deficiency leads to increased levels of ether-lipid species in hippocampus.*** Hippocampus from 8-month-old NRF2-null or wild-type background were extracted and submitted to untargeted lipidomics (n = 5 per genotype). A, PLS-DA representation of NRF2-WT and NRF2-KO hippocampal samples. B, Network analysis of reactions at the level of lipid subclass in the untargeted lipidomics in the NRF2-KO vs. NRF2-WT comparison. Weights in the edges represent individual Z-scores for the reactions. Gray edges represent reactions whose change is not significant (p-value >0.05) alone. Green and red edges represent reactions with a Z-score >1.645 (green, active reactions) or Z-score < −1.645 (red, suppressed reactions), corresponding to a p-value <0.05. Green and red shadows represent pathways of more than one reaction whose aggregated Z-score >1.645 or Z-score < −1.645, respectively. C, volcano plot shows dysregulated lipidic species in NRF2-KO relative to WT. The y-axis displays the negative logarithm (base 10) of the p-value, while the x-axis displays the logarithm (base 2) of the fold change. The p-value threshold is set to 0.05, and the log2(FC) ranges to (−0.5, 0.5). Significantly up- and down-regulated lipids are highlighted in orange and blue, respectively. D, Box-and-whisker plots showing the median, quartiles, and interquartile range of the indicated lipid intensity (k, means that the indicated values are multiplied by 1000). Statistical analysis was performed using Welch's *t*-test. **p < 0.01 vs. WT. E, mRNA levels of *Dhrs7b* and *VapA* genes. All mRNA levels were analyzed by qRT-PCR from brain samples from NRF2-WT (n = 8) and NRF2-KO (n = 7–8) and normalized by the levels of *Gapdh*, *Actb* and *Tbp*. Data are mean ± SEM. Statistical analysis was performed using the student's t-test. ***p < 0.001 vs. WT.

revealed that the conversion of phosphatidylethanolamine (PE) to phosphatidylserine (PS) was upregulated in the absence of NRF2 activity. Moreover, the 1-alkyl-2-acylglycerol (DG-O) conversion in 1-alkyl-2-acyl-*sn*-glycero-3-phosphorylethanolamine (PE-O) was significantly activated in NRF2-null mice compared to control mice (Fig. 2B). In the absence of NRF2, 17 lipid species were significantly altered in the hippocampus of NRF2-KO mice, as shown in the volcano and box plots (Fig. 2C and D and Suppl. Fig. 4C). Interestingly, 6 alkyl-lipid species were overrepresented in the hippocampus from NRF2-KO vs. NRF2-WT animals. The levels of the galactolipid MGDG O-16:2_3:0 and those of the alkyl-triglyceride TG O-18:1_16:1_18:1 were respectively down- or up-regulated by NRF2 absence (Fig. 2C and D). Among the alkyl-phospholipids upregulated in NRF2-KO vs. NRF2-WT, the three most abundant species were PE O-16:1_22:5; PE O-18:2_22:5 and PE O-18:1_22:5 characterized by a docosapentaenoic acid in their acyl chains. Moreover, hippocampi from NRF2-KO mice exhibited a significant increase in PE O-17:1_20:4, although it was less abundant than the previously mentioned species (Fig. 2C and D). The presence of an odd-chain alkyl moiety raises the possibility that this lipid may derive from an exogenous source, such as the gut microbiota or dietary components. Accordingly, the mRNA levels of two genes coding for enzymes involved in ether-lipids biosynthesis, *Dhrs7b* and *VapA*, were increased in brain samples from NRF2-null compared to control mice (Fig. 2E). Altogether these data support the fact that NRF2 deficiency disrupts the proportion of several lipid species, including increased alkyl-linked phospholipids in the hippocampus.

Alteration in lipid composition correlates with a reduction of hippocampal glutamatergic synapses in NRF2 deficient mice. The number of GABAergic and glutamatergic contacts was evaluated in hippocampi from NRF2-KO and NRF2-WT brains by immunofluorescence employing antibodies against the vGAT and vGLUT1 combined with Gephyrin and PSD95, respectively. We performed immunohistochemical analysis of three hippocampal areas, *Cornu ammonis* 1 and 2–3 (CA1 and CA2-3) and dentate gyrus (DG) and quantified synapses. As shown in Fig. 3A and B, the number of co-localizing puncta positive for vGAT/Gephyrin staining did not differ between both genotypes. Moreover, the density, intensity, or size of the vGAT or Gephyrin-stained puncta were also similar (Fig. 3C and D and Supp. Fig. 5A–D). However, the analysis of vGLUT1/PSD95 colocalization evidenced a reduction in the glutamatergic synaptic contacts in CA1 (Fig. 3E and F), which was concomitant with a reduction in the density of vGLUT1 (Fig. 3G) but not PSD95 (Fig. 3H). Evaluation of the size and intensity of vGLUT1 or PSD95 puncta did not retrieve any differences between genotypes (Supp. Fig. 5E–H). The decrease in synapse density could be due to decreased synapse formation or increased synapse elimination. Although we cannot exclude a contribution from synapses not being formed in NRF2 KO mice, the mice used were 6 months old and past the development phase of high rates of synapse formation. To assess whether NRF2 absence could have led to sustained microglial activation and excessive synaptic pruning, we evaluated the pattern of C1q, a complement protein recruited to synapses facilitating their engulfment by microglial cells [37]. As shown in Supp. Fig. 6A and 6C, while vGLUT1 was reduced in the hippocampus of NRF2-KO animals, neither the density nor the intensity of C1q puncta (Supp. Fig. 6B and 6F) or C1q/vGLUT1 colocalization (Supp. Fig. 6D and 6E) was affected by NRF2 expression. These results suggested that NRF2 modulates the levels of vGLUT1 and, therefore, participates in the maintenance of synaptic density, without altering synaptic pruning.

Crucial components of the vesicle machinery are reduced in presynaptic neurons due to NRF2 deficiency. Synaptosomes were isolated from the initial homogenate of hippocampal samples from 8-month-old NRF2-WT and NRF2-KO mice, then fractionated first into synaptosomal (Syn) and then further divided into synaptic vesicle (SV), and synaptosomal membrane (SM) fractions. Next, we evaluated synaptophysin (SYP), vGLUT1, and PSD95 protein levels by immunodetection. SYP levels, used as a control for total vesicle protein, were

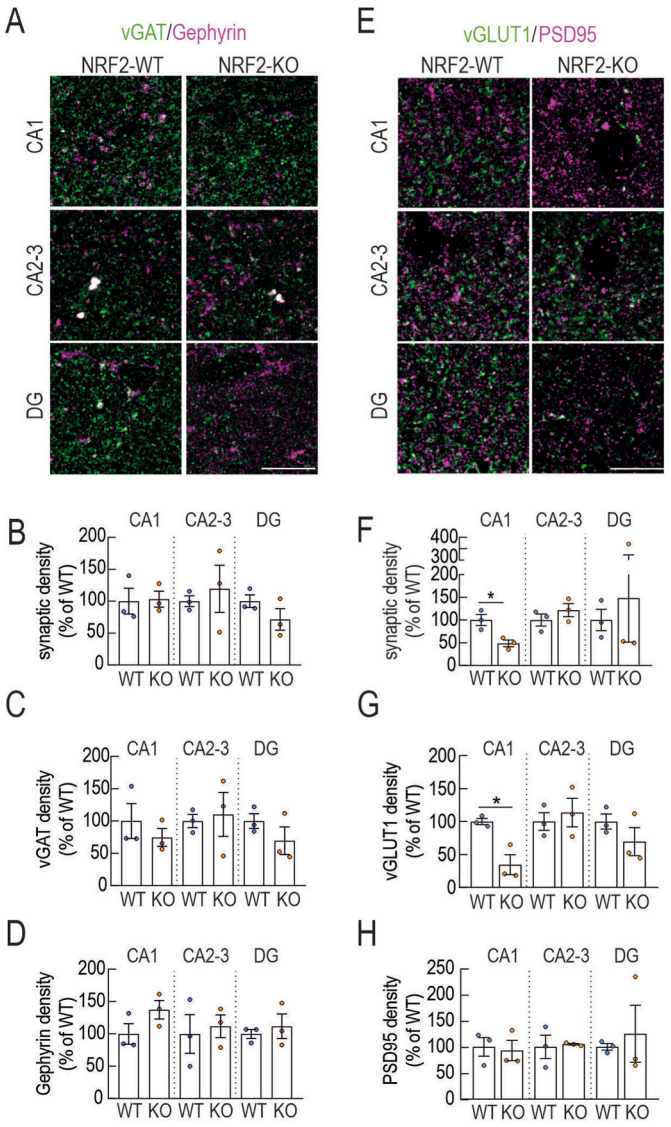

Fig. 3. ***The number of glutamatergic contacts is reduced in the hippocampus from NRF2-KO compared to NRF2-WT mice.*** A, confocal analysis of double immunofluorescence with anti-vGAT (green) and anti-Gephyrin (magenta) antibodies in brain slices from 6-month-old mice in a wild-type (NRF2-WT) or NRF2-null background (NRF2-KO). The scale bar corresponds to 10 μm. B, quantification of colocalization between vGAT and Gephyrin staining expressed and represented as synaptic density (number of puncta per 50 μm^2) and % of WT, respectively. C and D, quantification of either vGAT or Gephyrin density (number of puncta per 50 μm^2), respectively. E, confocal analysis of double immunofluorescence with anti-vGLUT1 (green) and PSD95 (magenta) antibodies in brain slices from 6-month-old mice in a wildtype (NRF2-WT) or NRF2-null background (NRF2-KO). The scale bar corresponds to 10 μm. F, quantification of colocalization between vGLUT1 and PSD95 staining expressed and represented as synaptic density and % of WT, respectively. G and H, quantification of either vGLUT1 or PSD95 density (number of puncta per 50 μm^2), respectively. The number of positive puncta was derived from 3 animals per genotype with an average of 3 fields per mouse. All data are mean ± SD. Statistical analysis was performed by using an unpaired *t*-test. *$p < 0.05$; **$p < 0.01$ vs. WT.

significantly enriched by 5-fold in the vesicular fraction (SV) relative to the initial homogenate (input) in NRF2-WT but only by 2-fold in NRF2-KO synaptosomes (Fig. 4A and B). Similarly, vGLUT1 levels showed approximately 60 % enrichment in the SV compared to the input sample in NRF2-WT, whereas this effect was absent in NRF2-KO mice (Fig. 4A and C). The reduction of SYP and vGLUT1 in NRF2-deficient samples

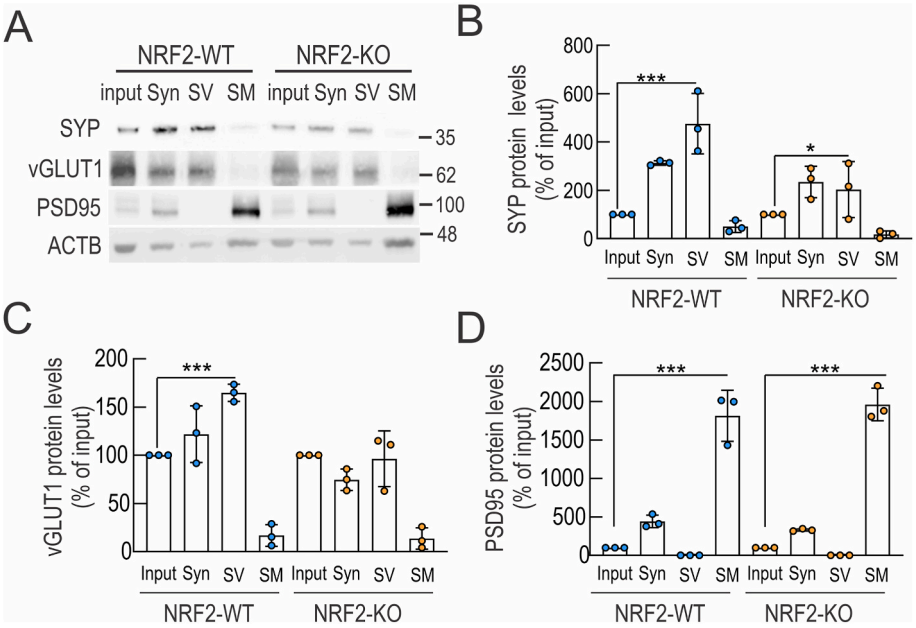

Fig. 4. ***NRF2 deficiency contributes to impairments in synaptosomal vesicle fractions.*** Synaptosomes were obtained from the initial homogenate of hippocampal preparations from 8-month-old NRF2-WT and NRF2-KO samples (Input), followed by fractionation into synaptosomal (Syn), synaptic vesicle (SV), and synaptosomal membrane (SM) fractions. A, immunoblots with specific antibodies as indicated in the panels. B, C and D, densitometric analysis of SYP, vGLUT1 or PSD95 relative to ACTB protein levels of representative blots from A. Data are mean ± SD (n = 3/genotype). Statistical analysis was performed using student's t-test to compare the input and the analyzed vesicular (B, C) or synaptosomal membrane (D) fractions considering *p < 0.05 and ***p < 0.001.

compared to WT suggests impaired synaptic composition, as a lower number of synapses could account for their decreased levels in the vesicular fraction, further supported by their overall reduction in the input. On the other hand, PSD95 protein levels were significantly enriched in the SM relative to input similarly in both genotypes (Fig. 4A and D). The lack of changes in SYP, vGLUT1, and PSD95 expression comparing samples from NRF2-KO and WT hippocampi (data not shown) suggests that NRF2 is unlikely to regulate these genes directly. We did not detect any changes in bulk glutamate levels in synaptosomal fractions by HPLC (data not shown). However, we cannot exclude additional contributions from defects in vesicle formation or trafficking in which lipids are significantly relevant. Altogether, these findings highlight the critical role of NRF2 in maintaining the integrity of the presynaptic vesicular compartment in the hippocampus, potentially linking the observed lipid alterations to synaptic dysfunction.

Ether lipids are enriched in synaptosomes from NRF2-deficient mice. To focus specifically on lipids within synapses, untargeted lipidomics was performed on synaptosome fractions from NRF2-KO vs. NRF2-WT mice. Although a relatively crude fractionation method was used, the synaptosome preparations are expected to be highly enriched in synaptic membranes. Nevertheless, contribution from other membranes sources, including mitochondrial and endoplasmic reticulum (Sup. Fig. 7A), should be considered. PCA plot was generated to check trends, and to ensure the grouping of all samples (PC1, 48.35 %; PC2, 25.36 %) (Sup. Fig. 7B). We detected 357 distinct lipid species detailed in Supp. Table 5. These categories were divided into six lipid classes (Suppl. Fig. 7C) containing 17 lipid species that were dysregulated upon NRF2 absence. Similarly to the whole hippocampus samples, PLS-DA revealed ether-PE among the top 25 contributing species to differentiating NRF2-WT and -KO synaptosomes (Suppl. Fig. 7D and Supp. Table 6). As shown in Fig. 5A, only the levels of PC-60:10 are reduced in NRF2-KO synaptosomes compared to WT. On the contrary, those of SM 18:1; O2/17:0 and Cer 17:1; O2/18:0 were up-regulated in the synaptosomes from NRF2-KO mice vs. control. Fourteen phospholipids species that appear up-regulated in NRF2-KO vs. WT synapses belong to PG (PG_17:0_17:0 and PG 22:5_22:6), PE (DMPE 18:0_22:6; PE 17:0_20:4; PE O 17:1_22:6; PE O 18:1_22:5 and PE P 18:0_22:5) and 5 PC (PC 15:0_16:0; PC 16:0_17:0; PC 16:0_17:1; PC 17:0_18:1 and PC 17:0_20:4) and PS (PS 17:0_22:6 and PS 18:0_22:5) families. The levels of four lipid species (PG 22:5_22:6, PE O-17:1_22:6, DMPE 18:0_22:6 and PS 17:0_22:6) which contain an acyl chain of docosahexaenoic acid (DHA, 22:6), are increased in the samples from NRF2-null mice (Fig. 5B and Suppl. Fig. 7E). Notably, two of the up-regulated lipids by NRF2 absence belong to the alkyl-PE family (PE O-18:1_22:5 and PE O-17:1_22:6) and one to the vinyl-PE group (PE P-18:0_22:5) (Fig. 5B). These results suggest that NRF2 deficiency disrupts the proportion of several lipid species, including 2 alkyl- and 1 vinyl-phospholipid species in hippocampal synapses.

Ether lipid precursor modifies the lipid composition of synapses. To investigate whether the high content of alkyl-lipids contributes to the reduction of glutamatergic contacts observed in NRF2-null mice, we established a neuronal model that modifies the lipid composition of synapses. This was achieved by treating primary neurons with the ether lipid precursor 1-O-hexadecyl-*sn*-glycerol (9 μM HG, 16 h) which integrates into the biosynthetic pathway upon phosphorylation by alkylglycerol kinase [38]. We treated neurons with a control compound, DL-α-palmitin (9 μM DP, 16 h), the fatty acyl analog of HG, to distinguish ether lipid-specific effects from those related to general lipid exposure. While HG is an ether lipid precursor, palmitin lacks the ether bond and serves as a structurally similar but functionally distinct lipid. Treatment with HG or DP at 9 μM did not reveal any toxic effects in neurons as measured by the MTT assay (data not shown). We performed lipidomics analyses of HG- and DP-synaptosome fractions from treated neurons to test if HG modifies the lipid composition of synapses. We quantified over 537 lipid species detailed in Supp. Table 7 and Supp. Fig. 8. As shown in Fig. 6A and B, one alkyl-linked glycerophosphoethanolamine (PE O-18:1_16:0) showed lower levels, while significantly higher levels were observed for six alkyl-linked glycerophosphocholines (PC O-30:0, PC O-31:0, PC O-32:0, PC O-16:0_16:0, PC O-15:2_18:2, and LPC O-16:0) and two alkyl-linked glycerophosphoethanolamines (PE O-16:1_20:4 and LPE O-16:0) in neurons treated with HG compared to those treated with DP. Furthermore, HG treatment also modifies the levels of some lipid species harboring the ether-bond and belonging to glycerophosphoinositols, diradylglycerols

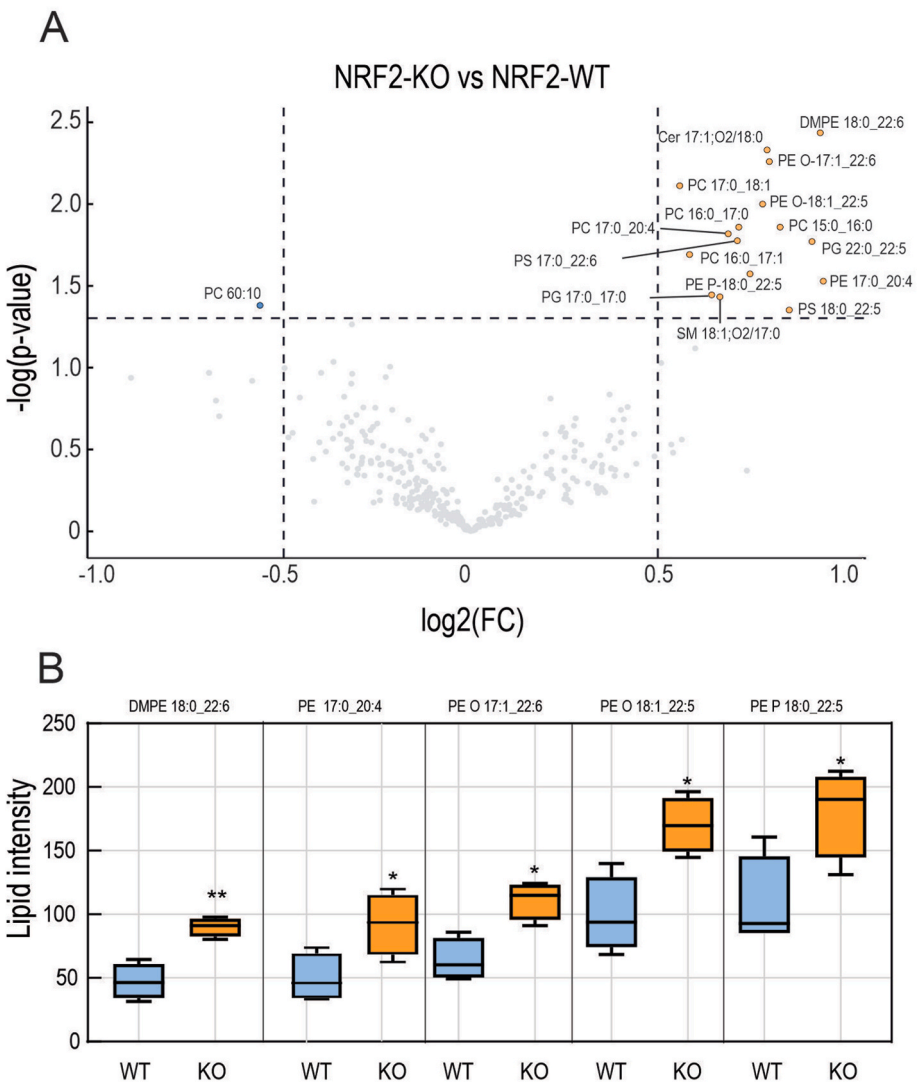

Fig. 5. ***NRF2 deficiency leads to ether-lipids accumulation in synaptosomes.*** Synaptosomes were obtained from the initial homogenate of hippocampal preparations from 8-month-old NRF2-WT or NRF2-KO samples followed by fractionation into synaptosomal fraction and subjected to untargeted lipidomics (n = 4 per genotype). A, Volcano plot shows dysregulated lipid species in a synaptosomal fraction from NRF2-KO relative to WT. The y-axis displays the negative logarithm (base 10) of the p-value, while the x-axis displays the logarithm (base 2) of the fold change. The p-value threshold is set to 0.05, and the log2(FC) ranges of (−0.5, 0.5). Significantly up- and down-regulated lipids are highlighted in orange and blue, respectively. B, Box-and-whisker plots showing the median lipid intensity, quartiles, and inter-quartile range. Statistical analysis was performed using Welch's *t*-test. *p < 0.05; **p < 0.01 vs. WT.

and triaradylglycerols families. Moreover, half of the most contributing species to PLS-DA were alkyl-linked (Supp. Fig. 8C and Supp. Table 8), confirming that synapses from neurons treated with HG were enriched in alkyl-lipids but not in vinyl-lipids (plasmalogens) compared to DP-treated cells.

HG reduced the density of vGLUT1/PSD95 positive contacts. Next, we determined the number of vGLUT1/PSD95 contacts in cortical/hippocampal primary neurons subjected to either 9 μM of DP or HG for 16h. Fig. 7A and B shows that the number of vGLUT1/PSD95-positive puncta was reduced by approximately 20 % in neurons treated with HG compared to DP-treated neurons. The reduction in synapse density in HG-treated neurons was accompanied by a decrease in the density and fluorescence intensity of vGLUT1 puncta (Fig. 7C), as well as a reduction in the intensity and size of PSD95 puncta compared to DP-treated neurons (Fig. 7D).

The HG effect on synaptic density was then analyzed in organotypic cultures, which preserve key aspects of the original tissue's structural and synaptic organization. Therefore, 300 μm-thick hippocampal slices were treated with either DP or HG (9 μM for 16h) and vGLUT1/PSD95 positive contacts were quantified. According to the previous results, the number of excitatory contacts in CA1 was reduced in HG-treated organotypic cultures compared to DP-treated slices (Fig. 7E and F). Interestingly, the HG effect reached a reduction in the number of excitatory contacts of approximately 80 % compared to DP-treated slices. Moreover, the alkyl-lipid precursor led to a profound reduction of both vGLUT1 and PSD95 density and intensity (Fig. 7G and H). These findings demonstrate a causal relationship between elevated alkyl-lipid levels and decreased glutamatergic contacts, potentially observed in NRF2-null mice. By employing a novel neuronal model to alter synaptic lipid composition, our findings bolster this connection, indicating that changes in lipids correlate with synapse loss.

Pharmacological activation of NRF2 prevented synaptic loss induced by HG. Next, we evaluated whether reinforcing NRF2 activity could be a potential strategy to prevent synaptic loss induced by the accumulation of alkyl-lipids in synapses. Both cortical/hippocampal neurons and organotypic cultures were treated with 6-(methylsulfinyl) hexyl isothiocyanate (6-MSITC or hexaraphane) (3 μM of 6 M for 4h) and then subjected to either HG or DP (9 μM for 16h). The strength of NRF2

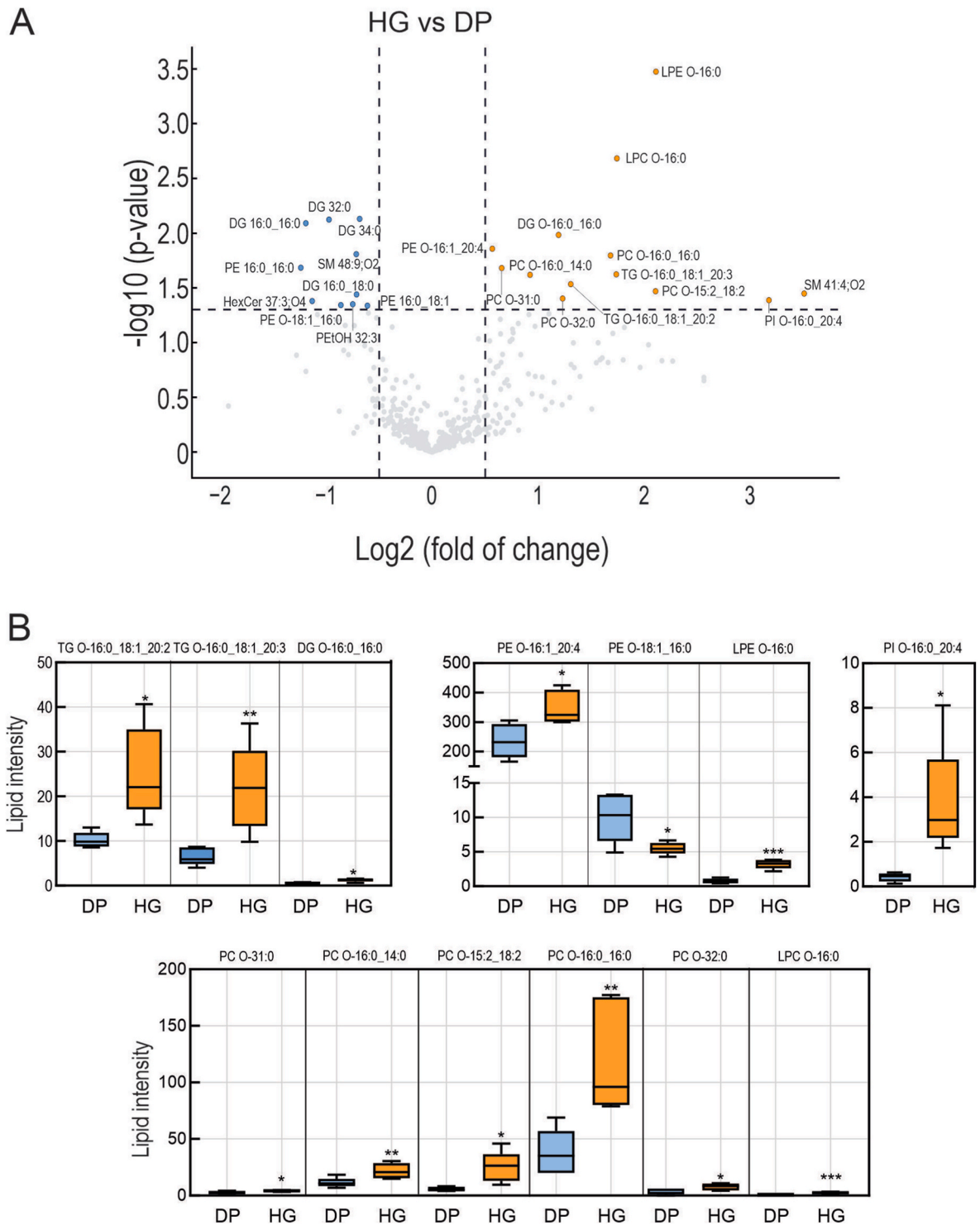

Fig. 6. ***HG treatment increased the levels of alkyl-lipids in synapses from primary neurons.*** Primary hippocampal/cortical neurons from mice maintained for 14 DIV were treated with either DL-α-palmitin (DP) or 1-*sn*-O-hexadecylglycerol (HG) (9 μM for 16h). Synaptosomes were obtained from the initial homogenate followed by fractionation into synaptosomal fraction and submitted to untargeted lipidomics (n = 5 per treatment). A, volcano plot shows dysregulated lipidic species in synaptosomal fraction from HG-relative to DP-treated neurons. The y-axis displays the negative logarithm (base 10) of the p-value, while the x-axis displays the logarithm (base 2) of the fold change. The p-value threshold is set to 0.05, and the log2(FC) ranges of (−0.5, 0.5). Significantly up- and down-regulated lipids are highlighted in orange and blue, respectively. B, Box-and-whisker plots showing the median lipid intensity, quartiles, and interquartile range. Statistical analysis was performed using Welch's *t*-test. *p < 0.05; **p < 0.01 vs. DP.

activation is evidenced by the increased levels of NRF2-protein detected in 6-MSITC-treated cultures compared to the control (Fig. 8A) [39]. In line with the previous results, HG treatment reduced the density of vGLUT1/PSD95-positive contacts in both systems, with a ~20 % reduction in primary neurons (Fig. 8B and C) and an 80 % reduction in hippocampal slices (Fig. 8D and E). Remarkably, cultures pretreated with 6-MSITC showed a complete restoration of synaptic contacts, even in hippocampal slices with a profound loss of vGLUT1/PSD95

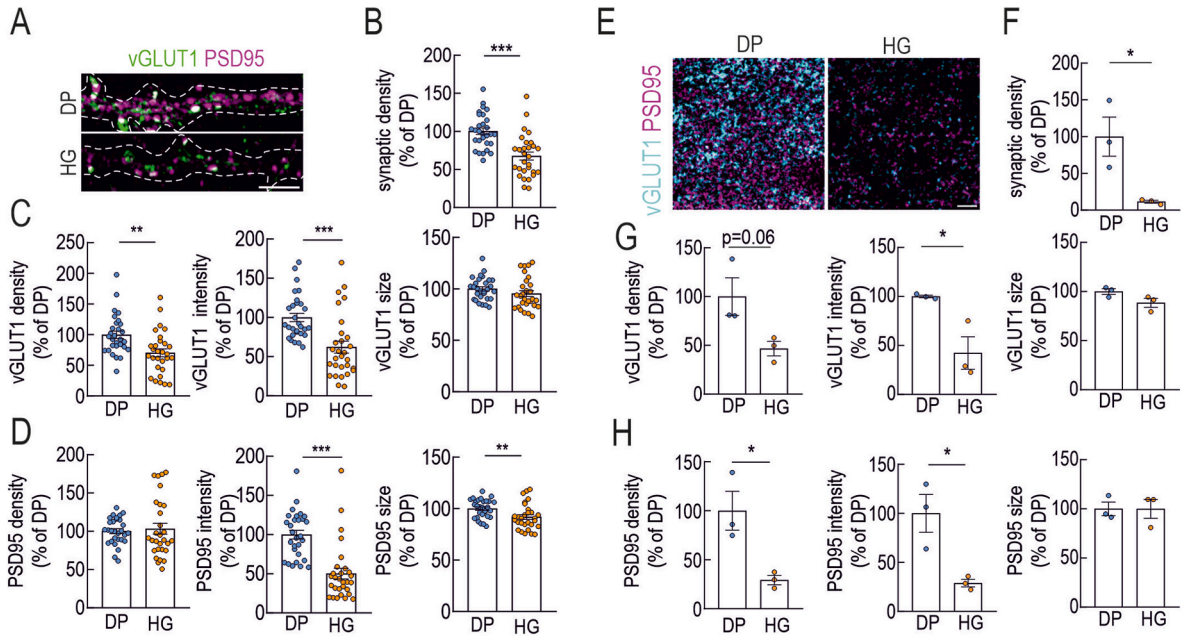

Fig. 7. ***Glutamatergic contacts are reduced in primary neurons and organotypic cultures submitted to an ether-lipid precursor.*** Primary hippocampal/cortical neurons (panels A–D) or 300 μm-thick hippocampal slices (panels E–H) from mice maintained for 14 DIV or 7 DIV, respectively, were treated with either DP or HG (9 μM for 16h). A and E, confocal analysis of double immunofluorescence with anti-vGLUT1 (green or blue) and PSD95 (magenta) antibodies in primary hippocampal/cortical neurons or organotypic cultures, respectively. The scale bar corresponds to 5 μm. B and F, quantification of colocalization between vGLUT1 and PSD95 staining expressed and represented as synaptic density and % of DP in primary hippocampal/cortical neurons or organotypic cultures, respectively. C and G, quantification of vGLUT1 puncta density (number of puncta per 50 μm^2), intensity and size represented as % of DP in primary hippocampal/cortical neurons or organotypic cultures, respectively. D and H, quantification of PSD95 puncta density (number of puncta per 50 μm^2), intensity and size represented as % of DP in primary hippocampal/cortical neurons or organotypic cultures, respectively. The number of positive puncta was derived from 3 independent experiments with an average of 30 neurons per treatment (A–D) or 3 images (E–H) and experiment. The data are mean ± SEM (A–D) or mean ± SD (E–H). Statistical analysis was performed using an unpaired *t*-test. *p < 0.05; **p < 0.01; ***p < 0.001 vs. DP.

colocalizing puncta (Fig. 8D and E). While the molecular mechanisms behind the observed synaptic restoration require further investigation, we can now, for the first time, connect the enhancement of endogenous defenses to the prevention of synaptic loss caused by disrupted lipid homeostasis.

4. Discussion

The involvement of NRF2 in synaptic function has long been proposed but never dissected before. In this work, we have sought to understand how NRF2 regulates synapses, describing its connection to alkyl-lipids and the effects these exert on synapses.

Previous studies have shown that the absence of NRF2 leads to reduced PSD95 levels in both primary neurons [23] and mouse models [21]. In contrast, our study only revealed decreased vGLUT1 expression, with no changes in PSD95. This discrepancy may be attributed to several experimental differences, such as the use of knockout versus CRISPR/-Cas9 approaches to suppress NRF2 expression [40], variations in the age or sex of the mice, or differences in the neuronal culture protocols. In agreement, we observed a decreased PSD95 density and intensity in organotypic cultures from NRF2-KO compared to NRF2-WT mice.

The number of glutamatergic contacts was reduced in the hippocampus of NRF2-KO mice compared to their wild-type counterparts. Additionally, vGLUT1 protein levels were also downregulated. This neurotransmitter transporter is essential for correct synaptic function and alterations in its levels are implicated in a variety of disorders, including schizophrenia [41], the age-related Parkinson's, or Alzheimer's diseases [42], where its downregulation has been correlated with cognitive decline [43,44]. vGLUT1 heterozygous animals show depressive-like behavior [45,46], which is a common feature shared by NRF2-deficient animals [47]. Interestingly, although mRNA levels of *Slc17a7* (coding gene of vGLUT1) were similar in both genotypes (data not shown), protein levels of presynaptic vGLUT1 were reduced in NRF2-deficient mice, suggesting the implication of post-translational modulation of vGLUT1 protein, which is still unknown, or as a result of an overall reduction of the number of synaptic vesicles. In line with this, electron microscopy of NRF2-KO mice presented reduced synaptic vesicles in CA1 [35], where we detected a reduction in vGLUT1 levels.

The timing of synaptic loss in the NRF2-deficient hippocampus is not directly addressed in this study. However, we selected 6-month-old-mice in which we previously showed to exhibit impaired LTP [18,24], indicating that synaptic dysfunction is already present. While this does not clarify whether deficits stem from impaired synapse formation or later degeneration, both are consistent with NRF2's role in maintaining neurogenic homeostasis. Supporting this, NRF2 regulates neural stem progenitor cell (NSPC) proliferation and neuronal differentiation, particularly during early postnatal stages and middle age [24,48]. Although our *in vitro* models link alkyl-lipids to synaptic density, they cannot resolve the developmental versus degenerative origin of the deficits. Still, our findings highlight the importance of NRF2-regulated lipid homeostasis in preserving synaptic integrity.

Synaptic refinement is necessary for the creation of new neuronal networks [37,49,50]. In the case of microglia, this interaction involves the complement proteins, such as C1q, and becomes aberrant in AD [37,51]. NRF2 activity prevents LPS- and TAU^{P301L}-induced neuroinflammation [52,53], and its absence is responsible for microgliosis after cerebral hypoperfusion [54]. Therefore, we hypothesized that NRF2 absence could be responsible for an aberrant microglial overactivation and subsequent synaptic engulfment. Nonetheless, the amount of C1q found in glutamatergic synapses was not different in the presence or absence of NRF2.

The brain has the second-highest lipid content in the human body, second only to adipose tissue. Brain lipids mainly consist of cholesterol, phospholipids, such as PC and PE, and sphingolipids [55]. Most sterols

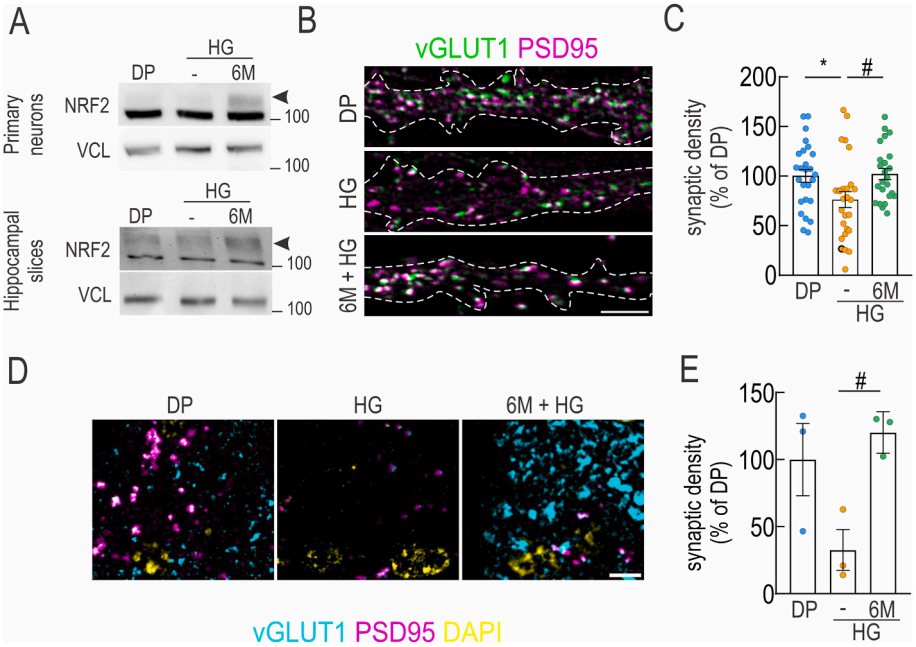

Fig. 8. ***Reinforcement of NRF2 activity prevents synaptic loss induced by the ether-lipids precursor.*** Primary hippocampal/cortical neurons (panels A, B and C) or 300 μm-thick hippocampal slices (panels A, D and E) from mice maintained for 14 DIV or 7 DIV, respectively, were pretreated with 6-MSITC (abbreviated here as 6 M) during 4h and then submitted to either DP or HG (9 μM for additional 16h). A, immunoblots with specific antibodies, as indicated in the panels. The arrowhead marks the band specific for NRF2 protein. VCL levels are used to control protein load per lane. B and D, confocal analysis of double immunofluorescence with anti-vGLUT1 (green or blue) and PSD95 (magenta) antibodies in primary hippocampal/cortical neurons or organotypic cultures, respectively. The scale bar corresponds to 5 μm. C and E, quantification of colocalization between vGLUT1 and PSD95 staining expressed and represented as synaptic density and % of DP in primary hippocampal/cortical neurons or organotypic cultures, respectively. The number of positive puncta was derived from 3 independent experiments with an average of 30 neurons per treatment (B and C) or 3 images (D and E) and experiment. The data are mean ± SEM (C) or mean ± SD (E). Statistical analysis was performed by using an unpaired *t*-test. *p < 0.05 vs. DP or #p < 0.05 vs. HG.

are synthesized within the brain mainly by astrocytes but also by neurons and are unable to cross the blood-brain barrier [56]. Although NRF2 has been linked to its metabolism through transcriptional activation of SREBP1c in hepatocytes [57], we did not detect significant changes in sterol species in the hippocampus or synaptosomes. Most saturated fatty acids (FA) are produced in the brain, still most of the polyunsaturated fatty acids (PUFAs) come from peripheral blood, with small amounts being synthesized by endothelial and astroglial cells [58–60]. The role of NRF2 in controlling the expression of genes related to FA metabolism, such as *Fas*, *Acc1, Scd-1c* and *Cd36,* has already been described in the context of the liver [61,62], but in the brain its role is still unknown. Evaluation of the lipid composition in NRF2-KO and WT brains revealed that over half of the dysregulated lipid species were phospholipids and that NRF2-deficiency was associated with the over-representation of four alkyl-lipid species in hippocampal samples, and with two alkyl- and one vinyl-lipid species in synaptosome fractions, respectively. Although a minor contribution from contaminating membranes, such as glial, mitochondrial, or other subcellular components, cannot be entirely ruled out due to the crude fractionation method used, the synaptic membranes might be the most represented membranes in the synaptosome samples [63]. Accordingly, the mRNA levels of two genes coding for enzymes involved in ether-lipid biosynthesis, *Dhrs7b* and *VapA*, were increased in brains from NRF2-null compared to control mice although protein levels or enzymatic activity are not addressed in this study. Mutations in other enzymes of the synthesis route, such as *Gnpat* or *Far1*, induce neurological disorders and neurotransmitter imbalance [64,65], hinting at the need for tight regulation of the levels of alkyl lipids in the brain. Altogether, these results emphasized the role of NRF2 modulating their levels in synapses in the hippocampus.

The specific function of the ether-lipid species up-regulated in synapses by NRF2 deficiency is currently unknown. Still the presence of either an alkyl- or an vinyl-bond and long-chain PUFAs at the *sn*-1 and *sn*-2 positions, respectively, allows us to hypothesize that they could share a structural role in membrane dynamics while contributing to oxidative stress regulation [66,67]. For instance, the up-regulation of the vinyl-PE (plasmalogen PE P-18:0_22:5) observed in NRF2-deficient animals may serve as a compensatory mechanism to counteract their increased susceptibility to oxidative stress [68]. Relevantly here, a study searching into the lipid composition of plasma from centenarians revealed an upregulation of alkyl-bonded and a downregulation of vinyl-bonded lipids, suggesting differences between these two similar lipids linked to healthier brain function [13].

Because ether-lipids have been described as either beneficial or toxic depending on their concentration and cellular context [69–72], we hypothesize that in contrast to the proposed antioxidant properties of vinyl-lipids (plasmalogens), some species of alkyl-lipids may contribute to the synaptic damage observed in NRF2-null animals. To test it, we employed the ether-lipid precursor 1-*O*-Hexadecyl-*sn*-glycerol (HG), which can enter the ether-lipid biosynthetic pathway [58,60,61]. We observed a deep modification of the lipid composition of synapses from HG vs. control-treated neurons consistent in an increase of alkyl lipids belonging to different lipid families, except for PE O-18:1_16:0, remarkably we were not able to detect any changes in vinyl-lipids (plasmalogens) species. Accordingly, HepG2 cells treated with 20 μM HG showed increased levels of ether-linked phospholipids (PE-O and PC-O) and a reduction in diacylglycerol (DG), consistent with ether lipid-driven remodeling. However, DP treatment also led to increases in ceramides and phosphatidylinositols, indicating that some lipidomic changes were not specific to ether lipids. This supports the use of DP as a relevant lipid control to parse out HG-specific effects from broader lipid-induced responses. However, differences in lipid classes may be due to tissue differences (neural vs. hepatic), differences in the doses, or even the species. The human and mouse lipidome are similar but not identical [73]. In our experiments, primary neurons subjected to HG

evidenced an up-regulation of two species of alkyl-PE (PE O-16:1_20:4 and LPE O-16:0) and three alkyl-PC (PC O-15:2_18:2; PC O-16:0_16:0 and PC O-16:0_14:0) that correlates with a reduction in the number of positive puncta for vGLUT1/PSD95. Although we are not able to specifically identify the same dysregulated lipidic species in synapses from both NRF2-null mice and HG-treated neurons, at least we can establish a correlation between higher alkyl-phospholipids levels and reduced vGLUT1/PSD95 positive contacts. Here, synapse density decreased by ~30 % in primary neurons treated with HG, with a greater reduction in organotypic cultures, likely due to the high astrocyte content and the involvement of other cell-specific metabolic routes. Astrocytes supply fatty acids and lipid precursors to neurons for membrane formation and synaptic function [74,75]. Therefore, they may fuel ether-lipid biosynthesis while also attempting to clear and degrade excess lipids from neurons. For instance, upon oxidative stress, peroxidized fatty acids are transported from neurons to astrocytes, via an ApoE-dependent mechanism to form lipid droplets and prevent neurodegeneration [75,76]. Although the molecular mechanism remains unexplored (e.g., NRF2-target genes involved, evaluation of possible off-target effects, analysis of ether-lipid enrichment in synapses), NRF2 activation by 6-MSITC restores the number of synaptic contacts lost due to HG, even in organotypic cultures, suggesting a crucial role for NRF2 in this process.

CRediT authorship contribution statement

Daniel Carnicero-Senabre: Writing – review & editing, Writing – original draft, Visualization, Validation, Methodology, Investigation, Formal analysis, Data curation, Conceptualization. **Mariana A. Barata:** Writing – review & editing, Methodology, Formal analysis. **José Jiménez-Villegas:** Writing – review & editing, Methodology, Formal analysis. **Claudia Guimas Almeida:** Writing – review & editing, Supervision, Resources, Funding acquisition. **Antonio Cuadrado:** Writing – review & editing, Writing – original draft, Visualization, Supervision, Resources, Project administration, Funding acquisition. **Ana I. Rojo:** Writing – review & editing, Writing – original draft, Visualization, Supervision, Resources, Project administration, Investigation, Funding acquisition, Formal analysis, Data curation, Conceptualization.

Fundings

This research was funded by the Spanish Ministry of Economy and Competitiveness (MINECO) (grants PID2019-110061RB-I00, PID-2021-122766OB-100 and PDC2022-133765-I00), Ramón Areces Foundation (2024_Rojo), CIBER -Consorcio Centro de Investigación Biomédica en Red-CB06/05/0010, Instituto de Salud Carlos III, Ministerio de Ciencia e Innovación, and The Autonomous Community of Madrid (grant P2022/BMD-7230). DCS holds an FPI contract of MICINN (Ministry of Science and Innovation, FPI-2020, PRE2020-091886). JJV holds an FPU PhD fellowship from the Spanish MIU (Ministry of Universities, FPU2020, FPU20/03326). This project has received funding (to CGA) from the Research Unit UID/04462: iNOVA4Health - Programa de Medicina Translacional and by the Associated Laboratory LS4FUTURE (LA/P/0087/2020), all financially supported by Fundação para a Ciência e Tecnologia (FCT)/Ministério da Educação, Ciência e Tecnologia and co-funded by FEDER under the PT2020 Partnership Agreement); CGA holds CEEC/iNOVA4Health contract (FCT); and MB holds an FCT doctoral fellowship (10.54499/2020.06758. BD). This article is based upon work from COST Action CA20121, supported by COST (European Cooperation in Science and Technology) (www.cost.eu) (https://benbedphar.org/about-benbedphar/).

Declaration of competing interest

The authors declare that they have no known competing financial interests or personal relationships that could have appeared to influence the work reported in this paper.

Acknowledgements

Authors thank Dr. M Martín (SEMOC, IIBM,CSIC) for her help in the acquisition of microscopy images.

Appendix A. Supplementary data

Supplementary data to this article can be found online at https://doi.org/10.1016/j.redox.2025.103853.

Data availability

No data was used for the research described in the article.

References

[1] F.J. Barrantes, Cognitive synaptopathy: synaptic and dendritic spine dysfunction in age-related cognitive disorders, Front. Aging Neurosci. 16 (2024 Oct 3) 1476909.
[2] R.D. Terry, E. Masliah, D.P. Salmon, N. Butters, R. DeTeresa, R. Hill, et al., Physical basis of cognitive alterations in Alzheimer's disease: synapse loss is the major correlate of cognitive impairment, Ann. Neurol. 30 (4) (1991 Oct) 572–580.
[3] J. Gu, L. Chen, R. Sun, J.L. Wang, J. Wang, Y. Lin, et al., Plasmalogens eliminate aging-associated synaptic defects and microglia-mediated neuroinflammation in mice, Front. Mol. Biosci. 9 (2022 Feb 23) 815320.
[4] J. Koch, K. Lackner, Y. Wohlfarter, S. Sailer, J. Zschocke, E.R. Werner, et al., Unequivocal mapping of molecular ether lipid species by LC-MS/MS in plasmalogen-deficient mice, Anal. Chem. 92 (16) (2020 Aug 18) 11268–11276.
[5] N.E. Braverman, A.B. Moser, Functions of plasmalogen lipids in health and disease, Biochim. Biophys. Acta 1822 (9) (2012) 1442–1452.
[6] J.M. Dean, I.J. Lodhi, Structural and functional roles of ether lipids, Protein Cell 9 (2) (2018) 196–206.
[7] S. Wallner, G. Schmitz, Plasmalogens the neglected regulatory and scavenging lipid species, Chem. Phys. Lipids 164 (6) (2011 Sep) 573–589.
[8] H. Goldfine, The appearance, disappearance and reappearance of plasmalogens in evolution, Prog. Lipid Res. 49 (4) (2010 Oct) 493–498.
[9] K. Huynh, R.N. Martins, P.J. Meikle, Lipidomic profiles in diabetes and dementia, J. Alzheimers Dis. JAD 59 (2) (2017) 433–444.
[10] P.J. Meikle, S.A. Summers, Sphingolipids and phospholipids in insulin resistance and related metabolic disorders, Nat. Rev. Endocrinol. 13 (2) (2017 Feb) 79–91.
[11] A. Broniec, R. Klosinski, A. Pawlak, M. Wrona-Krol, D. Thompson, T. Sarna, Interactions of plasmalogens and their diacyl analogs with singlet oxygen in selected model systems, Free Radic. Biol. Med. 50 (7) (2011) 892–898.
[12] B. Halliwell, Reactive oxygen species and the central nervous system, J. Neurochem. 59 (5) (1992) 1609–1623.
[13] I. Pradas, M. Jové, K. Huynh, J. Puig, M. Ingles, C. Borras, et al., Exceptional human longevity is associated with a specific plasma phenotype of ether lipids, Redox Biol. 21 (2019 Feb) 101127.
[14] A. Cuadrado, G. Manda, A. Hassan, M.J. Alcaraz, C. Barbas, A. Daiber, et al., Transcription factor NRF2 as a therapeutic target for chronic diseases: a systems medicine approach, Pharmacol. Rev. 70 (2) (2018) 348.
[15] J.H. Suh, S.V. Shenvi, B.M. Dixon, H. Liu, A.K. Jaiswal, R.M. Liu, et al., Decline in transcriptional activity of Nrf2 causes age-related loss of glutathione synthesis, which is reversible with lipoic acid, Proc. Natl. Acad. Sci. U. S. A. 101 (10) (2004 Mar 9) 3381–3386.
[16] N. Kubben, W. Zhang, L. Wang, T.C. Voss, J. Yang, J. Qu, et al., Repression of the antioxidant NRF2 pathway in premature aging, Cell 165 (6) (2016 Jun 2) 1361–1374.
[17] R. Strong, R.A. Miller, A. Antebi, C.M. Astle, M. Bogue, M.S. Denzel, et al., Longer lifespan in male mice treated with a weakly estrogenic agonist, an antioxidant, an α-glucosidase inhibitor or a Nrf2-inducer, Aging Cell 15 (5) (2016 Oct) 872–884.
[18] A.I. Rojo, M. Pajares, P. Rada, A. Nuñez, A.J. Nevado-Holgado, R. Killik, et al., NRF2 deficiency replicates transcriptomic changes in Alzheimer's patients and worsens APP and TAU pathology, Redox Biol. 13 (2017) 444.
[19] A. Cuadrado, Brain-protective mechanisms of transcription factor NRF2: toward a common strategy for neurodegenerative diseases, Annu. Rev. Pharmacol. Toxicol. 62 (2022 Jan 6) 255–277.
[20] J.P. McLin, O. Steward, Comparison of seizure phenotype and neurodegeneration induced by systemic kainic acid in inbred, outbred, and hybrid mouse strains, Eur. J. Neurosci. 24 (8) (2006 Oct) 2191–2202.
[21] J.Z. Xie, Y. Zhang, S.H. Li, H. Wei, H.L. Yu, Q.Z. Zhou, et al., P301S-hTau acetylates KEAP1 to trigger synaptic toxicity via inhibiting NRF2/ARE pathway: a novel mechanism underlying htau-induced synaptic toxicities, Clin. Transl. Med. 12 (8) (2022 Aug 2) e1003.
[22] T. Zeng, J. Li, L. Xie, Z. Dong, Q. Chen, S. Huang, et al., Nrf2 regulates iron-dependent hippocampal synapses and functional connectivity damage in depression, J. Neuroinflammation 20 (1) (2023) 212.
[23] J.A. Zweig, M. Caruso, M.S. Brandes, N.E. Gray, Loss of NRF2 leads to impaired mitochondrial function, decreased synaptic density and exacerbated age-related cognitive deficits, Exp. Gerontol. 131 (2020) 110767.

[24] N. Robledinos-Antón, A.I. Rojo, E. Ferreiro, Á. Núñez, K.H. Krause, V. Jaquet, et al., Transcription factor NRF2 controls the fate of neural stem cells in the subgranular zone of the hippocampus, Redox Biol. 13 (2017 Oct) 393–401.
[25] K. Itoh, T. Chiba, S. Takahashi, T. Ishii, K. Igarashi, Y. Katoh, et al., An Nrf2/small Maf heterodimer mediates the induction of phase II detoxifying enzyme genes through antioxidant response elements, Biochem. Biophys. Res. Commun. 236 (2) (1997) 313–322.
[26] H. Tsugawa, K. Ikeda, M. Takahashi, A. Satoh, Y. Mori, H. Uchino, et al., A lipidome atlas in MS-DIAL 4, Nat. Biotechnol. 38 (10) (2020 Oct) 1159–1163.
[27] C. Gaud, B. C Sousa, A. Nguyen, M. Fedorova, Z. Ni, V.B. O'Donnell, et al., BioPAN: a web-based tool to explore mammalian lipidome metabolic pathways on LIPID MAPS, F1000Research 10 (2021) 4.
[28] Z. Ni, M. Fedorova, LipidLynxX: a data transfer hub to support integration of large scale lipidomics datasets [Internet], bioRxiv (2020), p. 2020.04.09.033894. Available from: https://www.biorxiv.org/content/10.1101/2020.04.09.033894v2. (Accessed 6 May 2025).
[29] P. Shannon, A. Markiel, O. Ozier, N.S. Baliga, J.T. Wang, D. Ramage, et al., Cytoscape: a software environment for integrated models of biomolecular interaction networks, Genome Res. 13 (11) (2003 Nov) 2498–2504.
[30] F.S. Mirfakhar, J. Castanheira, R. Domingues, J.S. Ramalho, C.G. Almeida, The alzheimer's disease risk gene CD2AP functions in dendritic spines by remodeling F-Actin, J. Neurosci. 44 (48) (2024 Nov 27). Available from: https://www.jneurosci.org/content/44/48/e1734232024. (Accessed 14 May 2025).
[31] L. Stoppini, P.A. Buchs, D. Muller, A simple method for organotypic cultures of nervous tissue, J. Neurosci. Methods 37 (2) (1991 Apr) 173–182.
[32] A.I. Rojo, N.G. Innamorato, A.M. Martín-moreno, M.L.D. Ceballos, M. Yamamoto, A. Cuadrado, Nrf2 regulates microglial dynamics and neuroinflammation in experimental Parkinson's disease, Glia 58 (5) (2010) 588.
[33] T. Burrinha, C. Cunha, M.J. Hall, M. Lopes-da-Silva, M.C. Seabra, C. Guimas Almeida, Deacidification of endolysosomes by neuronal aging drives synapse loss, Traffic Cph. Den. 24 (8) (2023 Aug) 334–354.
[34] A. Muto, M. Ohkura, G. Abe, J. Nakai, K. Kawakami, Real-time visualization of neuronal activity during perception, Curr. Biol. 23 (4) (2013) 307.
[35] R. Zhang, Y. Gao, Y. Li, D. Geng, Y. Liang, Q. He, et al., Nrf2 improves hippocampal synaptic plasticity, learning and memory through the circ-Vps41/miR-26a-5p/CaMKIV regulatory network, Exp. Neurol. 351 (2022) 113998.
[36] R.M. Lazarenko, C.E. DelBove, Q. Zhang, Fluorescent measurement of synaptic activity using FM dyes in dissociated hippocampal cultured neurons, Bio-Protoc. 8 (2) (2018 Jan 20) e2690.
[37] S. Hong, L. Dissing-Olesen, B. Stevens, New insights on the role of microglia in synaptic pruning in health and disease, Curr. Opin. Neurobiol. 36 (2016) 128–134.
[38] N. Nagan, R.A. Zoeller, Plasmalogens: biosynthesis and functions, Prog. Lipid Res. 40 (3) (2001 May) 199–229.
[39] A. Kopacz, A.I. Rojo, C. Patibandla, D. Lastra-Martínez, A. Piechota-Polanczyk, D. Kloska, et al., Overlooked and valuable facts to know in the NRF2/KEAP1 field, Free Radic. Biol. Med. 192 (2022 Nov 1) 37–49.
[40] M.A. El-Brolosy, D.Y.R. Stainier, Genetic compensation: a phenomenon in search of mechanisms, PLoS Genet. 13 (7) (2017) e1006780.
[41] A. Oni-Orisan, L.V. Kristiansen, V. Haroutunian, J.H. Meador-Woodruff, R. E. McCullumsmith, Altered vesicular glutamate transporter expression in the anterior cingulate cortex in schizophrenia, Biol. Psychiatry 63 (8) (2008) 766–775.
[42] A. Kashani, C. Betancur, B. Giros, E. Hirsch, S.E. Mestikawy, Altered expression of vesicular glutamate transporters VGLUT1 and VGLUT2 in Parkinson disease, Neurobiol. Aging 28 (4) (2007) 568–578.
[43] M. Rodriguez-Perdigon, R.M. Tordera, F.J. Gil-Bea, G. Gerenu, M.J. Ramirez, M. Solas, Down-regulation of glutamatergic terminals (VGLUT1) driven by Aβ in Alzheimer's disease, Hippocampus 26 (10) (2016 Oct) 1303–1312.
[44] O.W.G. Wood, J. Walby, J.H. Yeung, S. Ke, T.H. Palpagama, C. Turner, et al., Alzheimer's disease-associated region-specific decrease of vesicular glutamate transporter immunoreactivity in the medial temporal lobe and superior temporal gyrus, Neuroscience 546 (2024 May 14) 75–87.
[45] R.M. Tordera, S. Totterdell, S.M. Wojcik, N. Brose, N. Elizalde, B. Lasheras, et al., Enhanced anxiety, depressive-like behaviour and impaired recognition memory in mice with reduced expression of the vesicular glutamate transporter 1 (VGLUT1), Eur. J. Neurosci. 25 (1) (2007) 281–290.
[46] S.M. Wojcik, J.S. Rhee, E. Herzog, A. Sigler, R. Jahn, S. Takamori, et al., An essential role for vesicular glutamate transporter 1 (VGLUT1) in postnatal development and control of quantal size, Proc. Natl. Acad. Sci. U. S. A. 101 (18) (2004 May 4) 7158–7163.
[47] M.D. Martín-de-Saavedra, J. Budni, M.P. Cunha, V. Gómez-Rangel, S. Lorrio, L. D. Barrio, et al., Nrf2 participates in depressive disorders through an anti-inflammatory mechanism, Psychoneuroendocrinology 38 (10) (2013) 2010–2022.
[48] S. Ray, M.J. Corenblum, A. Anandhan, A. Reed, F.O. Ortiz, D.D. Zhang, et al., A role for Nrf2 expression in defining the aging of hippocampal neural stem cells, Cell Transplant. 27 (4) (2018 Apr) 589–606.
[49] D.W. Chung, Z.P. Wills, K.N. Fish, D.A. Lewis, Developmental pruning of excitatory synaptic inputs to parvalbumin interneurons in monkey prefrontal cortex, Proc. Natl. Acad. Sci. U. S. A. 114 (4) (2017) E629–E637.
[50] M.È. Tremblay, R.L. Lowery, A.K. Majewska, Microglial interactions with synapses are modulated by visual experience, PLoS Biol. 8 (11) (2010 Nov 2) e1000527.
[51] B. Dejanovic, T. Wu, M.C. Tsai, D. Graykowski, V.D. Gandham, C.M. Rose, et al., Complement C1q-dependent excitatory and inhibitory synapse elimination by astrocytes and microglia in Alzheimer's disease mouse models, Nat. Aging 2 (9) (2022 Sep) 837–850.
[52] N.G. Innamorato, A.I. Rojo, Á.J. García-Yagüe, M. Yamamoto, M.L. de Ceballos, A. Cuadrado, The transcription factor Nrf2 is a therapeutic target against brain Inflammation 1, J. Immunol. 181 (1) (2008 Jul 1) 680–689.
[53] I. Lastres-Becker, N.G. Innamorato, T. Jaworski, A. Rábano, S. Kügler, F. Van Leuven, et al., Fractalkine activates NRF2/NFE2L2 and heme oxygenase 1 to restrain tauopathy-induced microgliosis, Brain J. Neurol. 137 (Pt 1) (2014 Jan) 78–91.
[54] A.F. Hubbs, S.A. Benkovic, D.B. Miller, J.P. O'Callaghan, L. Battelli, D. Schwegler-Berry, et al., Vacuolar leukoencephalopathy with widespread astrogliosis in mice lacking transcription factor Nrf2, Am. J. Pathol. 170 (6) (2007) 2068–2076.
[55] A. Naudí, R. Cabré, M. Jové, V. Ayala, H. Gonzalo, M. Portero-Otín, et al., Lipidomics of human brain aging and Alzheimer's disease pathology, Int. Rev. Neurobiol. 122 (2015) 133–189.
[56] U. Jin, S.J. Park, S.M. Park, Cholesterol metabolism in the brain and its association with parkinson's disease, Exp. Neurobiol. 28 (5) (2019 Oct 31) 554–567.
[57] P.C. Shimpi, V.R. More, M. Paranjpe, A.C. Donepudi, J.M. Goodrich, D.C. Dolinoy, et al., Hepatic lipid accumulation and Nrf2 expression following perinatal and peripubertal exposure to bisphenol A in a mouse model of nonalcoholic liver disease, Environ. Health Perspect. 125 (8) (2017 Aug 16) 087005.
[58] S.A. Moore, Polyunsaturated fatty acid synthesis and release by brain-derived cells in vitro, J. Mol. Neurosci. MN 16 (2–3) (2001) 195–200. ; discussion 215-221.
[59] F. Pifferi, B. Laurent, M. Plourde, Lipid transport and metabolism at the blood-brain interface: implications in health and disease, Front. Physiol. 12 (2021) 645646.
[60] J.H. Yoon, Y. Seo, Y.S. Jo, S. Lee, E. Cho, A. Cazenave-Gassiot, et al., Brain lipidomics: from functional landscape to clinical significance, Sci. Adv. 8 (37) (2022 Sep 16) eadc9317.
[61] A. Cuadrado, S. Kügler, I. Lastres-Becker, Pharmacological targeting of GSK-3 and NRF2 provides neuroprotection in a preclinical model of tauopathy, Redox Biol. 14 (2018) 522–534.
[62] T. Kamisako, Y. Tanaka, Y. Kishino, T. Ikeda, K. Yamamoto, S. Masuda, et al., Role of Nrf2 in the alteration of cholesterol and bile acid metabolism-related gene expression by dietary cholesterol in high fat-fed mice, J. Clin. Biochem. Nutr. 54 (2) (2014 Mar 1) 90–94.
[63] P.R. Dunkley, P.J. Robinson, Synaptosome preparations: which procedure should I use? in: K.M. Murphy (Ed.), Synaptosomes [Internet] Springer, New York, NY, 2018, pp. 27–53, https://doi.org/10.1007/978-1-4939-8739-9_3. (Accessed 21 May 2025).
[64] F. Dorninger, T. König, P. Scholze, M.L. Berger, G. Zeitler, C. Wiesinger, et al., Disturbed neurotransmitter homeostasis in ether lipid deficiency, Hum. Mol. Genet. 28 (12) (2019) 2046–2061.
[65] S. Ferdinandusse, K. McWalter, H.T. Brinke, L. Ijlst, P.M. Mooijer, J.P.N. Ruiter, et al., An autosomal dominant neurological disorder caused by de novo variants in FAR1 resulting in uncontrolled synthesis of ether lipids, Genet Med. Off. J. Am Coll. Med. Genet 23 (4) (2021) 740–750.
[66] Z. Chen, I.L. Ho, M. Soeung, E.Y. Yen, J. Liu, L. Yan, et al., Ether phospholipids are required for mitochondrial reactive oxygen species homeostasis, Nat. Commun. 14 (1) (2023) 2194.
[67] H.K. Mangold, N. Weber, Biosynthesis and biotransformation of ether lipids, Lipids 22 (11) (1987 Nov 1) 789–799.
[68] H. Motohashi, M. Yamamoto, Nrf2-Keap1 defines a physiologically important stress response mechanism, Trends Mol. Med. 10 (11) (2004) 549–557.
[69] J. Bergan, T. Skotland, T. Sylvänne, H. Simolin, K. Ekroos, K. Sandvig, The ether lipid precursor hexadecylglycerol causes major changes in the lipidome of HEp-2 cells, PLoS One 8 (9) (2013) e75904.
[70] L. Diomede, B. Piovani, E.J. Modest, A. Noseda, M. Salmona, Increased ether lipid cytotoxicity by reducing membrane cholesterol content, Int. J. Cancer 49 (3) (1991) 409–413.
[71] P. Brites, A.S. Ferreira, TF da Silva, V.F. Sousa, A.R. Malheiro, M. Duran, et al., Alkyl-glycerol rescues plasmalogen levels and pathology of ether-phospholipid deficient mice, PLoS One 6 (12) (2011) e28539.
[72] R.A. Zoeller, T.J. Grazia, P. LaCamera, J. Park, D.P. Gaposchkin, H.W. Farber, Increasing plasmalogen levels protects human endothelial cells during hypoxia, Am. J. Physiol. Heart Circ. Physiol. 283 (2) (2002) 671.
[73] R.B. Chan, T.G. Oliveira, E.P. Cortes, L.S. Honig, K.E. Duff, S.A. Small, et al., Comparative lipidomic analysis of mouse and human brain with Alzheimer disease, J. Biol. Chem. 287 (4) (2012) 2678–2688.
[74] C.N. Barber, D.M. Raben, Lipid metabolism crosstalk in the brain: glia and neurons, Front Cell Neurosci. 13 (2019 May 21). Available from: https://www.frontiersin.org/journals/cellular-neuroscience/articles/10.3389/fncel.2019.00212/full. (Accessed 4 March 2025).
[75] M.S. Ioannou, J. Jackson, S.H. Sheu, C.L. Chang, A.V. Weigel, H. Liu, et al., Neuron-astrocyte metabolic coupling protects against activity-induced fatty acid toxicity, Cell 177 (6) (2019) 1522–1535.e14.
[76] M.J. Moulton, S. Barish, I. Ralhan, J. Chang, L.D. Goodman, J.G. Harland, et al., Neuronal ROS-induced glial lipid droplet formation is altered by loss of Alzheimer's disease-associated genes, Proc. Natl. Acad. Sci. U. S. A 118 (52) (2021) e2112095118.